Exploring Bethe–Salpeter Excited-State Dipoles: The Challenging Case of Increasingly Long Push–Pull Oligomers

Iryna Knysh, Jose Villalobos-Castro, Ivan Duchemin, Xavier Blase, Denis Jacquemin

Exploring Bethe-Salpeter Excited States Dipoles : the Challenging Case of Increasingly Long Push-Pull Oligomers

Iryna Knysh,[†] Jose D. J. Villalobos-Castro,[‡] Ivan Duchemin,[‡] Xavier Blase,[*,¶] and Denis Jacquemin[*,†,§]

†*Nantes Université, CNRS, CEISAM UMR 6230, F-44000 Nantes, France*

‡*Université Grenoble Alpes, CEA, IRIG-MEM-L Sim, 38054 Grenoble, France*

¶*Université Grenoble Alpes, CNRS, Institut NEEL, F-38042 Grenoble, France*

§*Institut Universitaire de France, 75005 Paris, France*

E-mail: xavier.blase@neel.cnrs.fr; Denis.Jacquemin@univ-nantes.fr

Abstract

The change of molecular dipole moment induced by photon absorption is key to interpret the measured optical spectra. Except for compact molecules, time-dependent density functional theory (TD-DFT) remains the only theory allowing to quickly predict μ^{ES}, albeit with a strong dependency on the selected exchange-correlation functional. This Letter presents the first assessment of the performances of the many-body Green's function Bethe-Salpeter equation (BSE) formalism for the evaluation of the μ^{ES}. We explore increasingly long push-pull oligomers as they present an excited-state nature evolving with system size. This work shows that BSE's μ^{ES} do present the same evolution with oligomeric length as their CC2 and CCSD counterparts, with a dependency on the starting exchange-correlation functional that is strongly decreased as compared to TD-DFT. This Letter demonstrates that BSE is a valuable alternative to TD-DFT for properties related to the excited-state density, and not only for transition energies and oscillator strengths.

Graphical TOC Entry

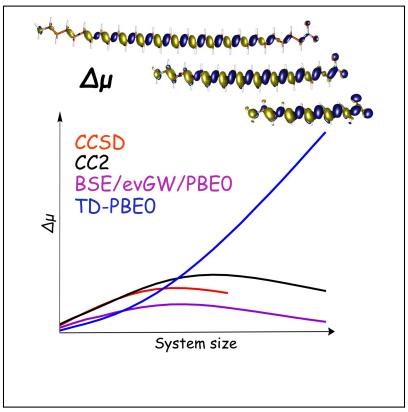

The permanent dipole moment (μ) stands as one of the most important molecular feature, as it is directly related to key properties of matter, e.g., the strength of intermolecular interactions with other derivatives, the solubility of the compound, the molecular orientation in a laser field, etc. Obtaining non-null μ requires an asymmetric distribution of the electric charges constituting the system, hence a non-centrosymmetric molecular structure, which can be guaranteed by an appropriate chemical substitution. If a molecule is promoted from its ground electronic state (GS) to one of its excited states (ES), e.g., by photon absorption, it can undergo drastic variations of its dipole moment. When the ES dipole (μ^{ES}) is significantly larger than its GS counterpart (μ^{GS}), that is when the excess dipole ($\Delta\mu$, see Eq. 1) is positive, the absorption spectrum is characterized by positive solvatochromism and the emission becomes often quenched in very polar solvents. Accurately quantifying $\Delta\mu$ and μ^{ES} unfortunately remains challenging for both experiment and theory. Experimentally, μ^{ES} are indirectly accessed either through Stark effect measurements or solvatofluorochromism determinations. In the former, one measures the variations of the position and topologies of the vibronic signatures under an external electric field, and such approach can be applied to very small compounds in gas phase only, and remains far from error-free.[1–3] In the solvatofluorochromic approach, one studies the changes of the position of the fluorescence maximum in solvent of various polarities and deduce μ^{ES} using the Lippert-Mataga equation, an approach that comes with significant simplifications and a rather large incertitude.[1] This is why most μ^{ES} are theoretically determined. However, the first-principle calculations of μ^{ES} requires either performing numerical derivatives (finite-field approach) or applying a level of theory delivering the ES density. Both strategies are demanding, limiting the palette of approaches actually applicable in realistic cases. Amongst the single-reference approaches developed for ES calculations, time-dependent density functional theory (TD-DFT)[4–6] remains the main workhorse and this general statement holds for μ^{ES}. Whilst the ES TD-DFT densities can be efficiently obtained through the so-called Z-vector approach,[7,8] the μ^{ES} can be quite inaccurate and/or strongly dependent upon the selected exchange-correlation functional (XCF),[3,8–15] with XCF trends often harder to rationalize than for energies. In this context, we note that μ^{GS} has been used by the Head-Gordon's group as a handy metric for probing the quality of the DFT GS densities provided by various XCF,[16,17] and such a strategy is obviously relevant for the ES (TD-DFT) as well. As TD-DFT μ^{ES} are not always reliable, it seems natural to turn towards wave function approaches, and the second-order coupled cluster (CC2)[18] and algebraic diagrammatic construction [ADC(2)] methods[19,20] directly come to mind, as they are likely the only two wave function methods allowing calculations on medium-sized molecules. If these approaches are by construction free of XCF-bias, they

scale less favorably with system size than TD-DFT and, as can be deduced from previous benchmarks, are far from chemically accurate.[3,21–23] In addition several models have been developed for calculating μ^{ES} at a given ADC or CC level. First, one can apply a rigorous Lagrangian formalism in the so-called linear-response (LR) approach, that can be applied to both CC2 and ADC(2).[18,24–29] Yet one should still select between the orbital-unrelaxed and orbital-relaxed approaches, the former bypassing the determination of the impact of the electric field on the orbital response.[30,31] Alternatively to LR, one can use the so-called intermediate state representation (ISR)[20,32,33] for ADC approaches or the equation-of-motion (EOM) method[34,35] for CC theories. In EOM, in contrast to LR, one freezes the ground-state CC amplitudes during the calculation.[35,36] Discussion of the actual impact of these changes can be found elsewhere.[3,22] We recall that while the LR and EOM (or ISR) properties such as dipoles differ, these approaches yield the same transition energies (ΔE).

The many-body Green's function Bethe-Salpeter equation (BSE) formalism,[37–46] relying on input *GW*[47–51] quasiparticle energies, offers an alternative to the above mentioned approaches. Interestingly, it presents the same scaling with system size as TD-DFT but accurately captures electron-hole interactions, which is advantageous for evaluating ES, especially when significant charge-transfer (CT) is at play,[52–56] that is when there is a significant density change between the GS and the ES. Many assessments of the BSE/*GW* transition energies, performed with different flavors of this theory and with various molecular sets have clearly demonstrated the advantages of this approach as compared to TD-DFT.[57–67] Notably, when a partially self-consistent *GW* approach is used, generally noted ev*GW*,[68–70] BSE/*GW* transition energies are almost independent of the starting XCF. If one could state that the *pros* and *cons* of BSE/*GW* for excitation energies are now well-assessed, much less is known for properties, a logical consequence of the lack of analytical gradients at this level of theory. We are aware of a detailed benchmark of a key transition property, i.e., the oscillator strength (f),[71] as well as a few studies of ES geometries performed on compact molecules relying on numerical forces[72,73] or using approximate analytic derivatives,[74] or exploring a reduced dimensionality potential energy surface for medium size molecules.[75–77] If these studies have generally concluded that BSE/*GW* yields accurate data, there is to the very best of our knowledge, no previous investigation of μ^{ES} at the BSE/*GW* level and the present Letter is a first answer to this gap.

To this end, we have selected α,ω-amino-nitro-polyene chains (Figure 1), that offer, as demonstrated below, a stringent methodological test for ES theories. Let us start by investigating the evolution with N of the properties as described by wave function approaches. The results for $\Delta\mu$ are displayed in Figure 2, whereas graphs for transition energies, oscillator strength, μ^{GS}, and μ^{ES}, as well as list of numerical values can be

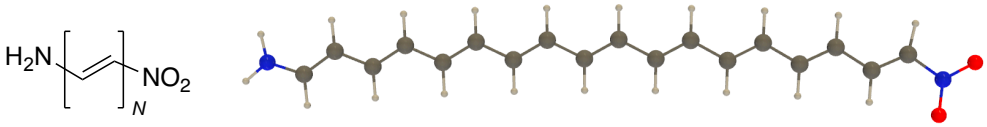

Figure 1: Left: scheme of the oligomers under investigation, with N, the number of double bonds going from 1 to 20. Right: optimal geometry to the nonamer (N=9) that presents the largest $\Delta\mu$ according to EOM-CCSD/cc-pVDZ calculations.

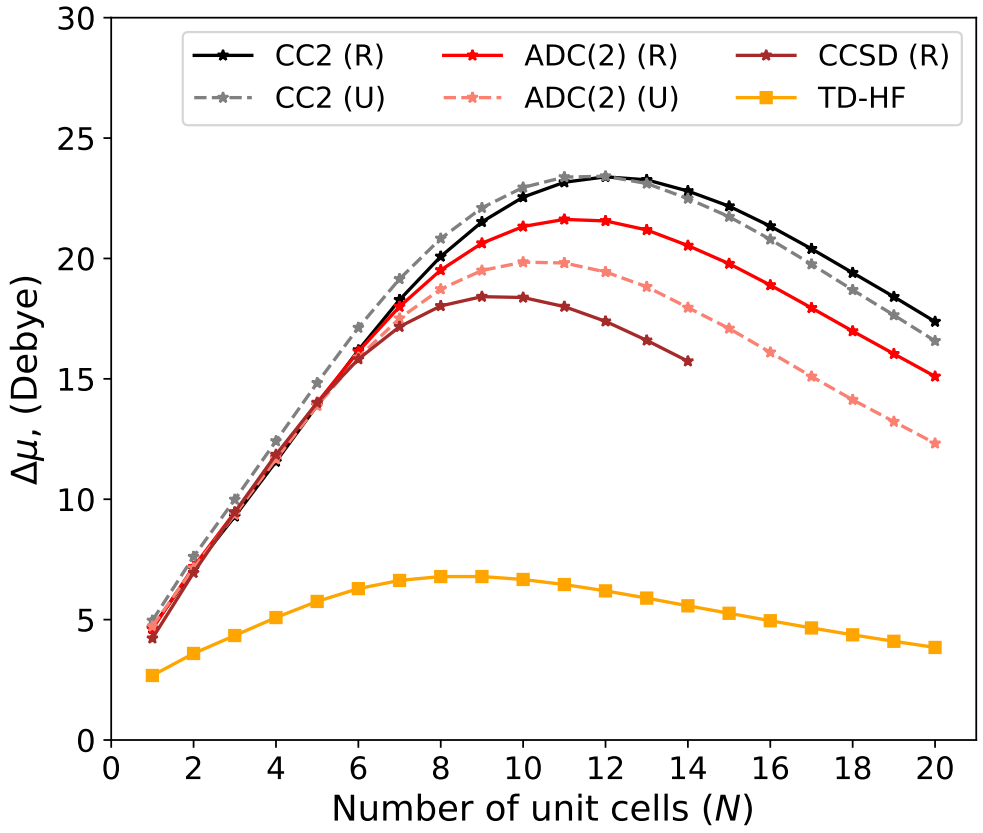

Figure 2: Evolution with N of the excess dipole moment. All values are in Debye and have been determined with the cc-pVTZ atomic basis set but the EOM-CCSD one for which cc-pVDZ is used. R and U stand for the relaxed and unrelaxed approaches.

found in the SI. Briefly, ΔE constantly decreases with increasing N for all approaches, slowly converging for the longer chains, whereas the associated f steadily increases as chain lengthens. For these properties, ADC(2) and CC2 values are extremely close, whereas the CCSD transition energies are larger than the CC2 ones, which is an expected trend.[78]

With all wave function schemes, the μ^{GS} rapidly increases in going from N=1 to ca. N=10, and then saturates to values between 10 and 15 Debye (D) for ADC(2), CC2, and CCSD (see Figure S1 in the SI). Globally, μ^{ES} behaves as $\Delta\mu$ discussed below. All curves shown in Figure 2 share the same general topology: as the chain lengthens $\Delta\mu$ first rapidly increases, then reach a maximum before slowly decreasing. The

differences between the unrelaxed and relaxed LR-ADC(2) and LR-CC2 results are small and we discuss only the latter in the following. One notices that the ADC(2) and CC2 values are almost equivalent for short chains, whereas the ADC(2) values are slightly smaller for longer chains. At the CC2 level, $\Delta\mu$ peaks at 23.4 D for $N = 12$, the maximum being reach one unit earlier ($N = 11$) with ADC(2). As can be seen in the SI, the μ^{ES} maxima also are similar with both theories, 33.9 D at N=12 for ADC(2) and 37.7 D at $N = 13$ for CC2. The EOM-CCSD calculations are only achievable with a more compact basis set (see Figure S2 in the SI for a comparison between double- and triple-ζ CCSD results on small chains, showing comparable trends, with a slight exaggeration of $\Delta\mu$ with cc-pVDZ), but clearly deliver a faster saturation with a maximal $\Delta\mu$ of 18.4 D reached for N=9. Finally, the TD-HF approach provides a qualitatively correct evolution, but with strongly underestimated absolute values, slightly too early maxima for both $\Delta\mu$ and μ^{ES}, and too sluggish decreases for the longest chains.

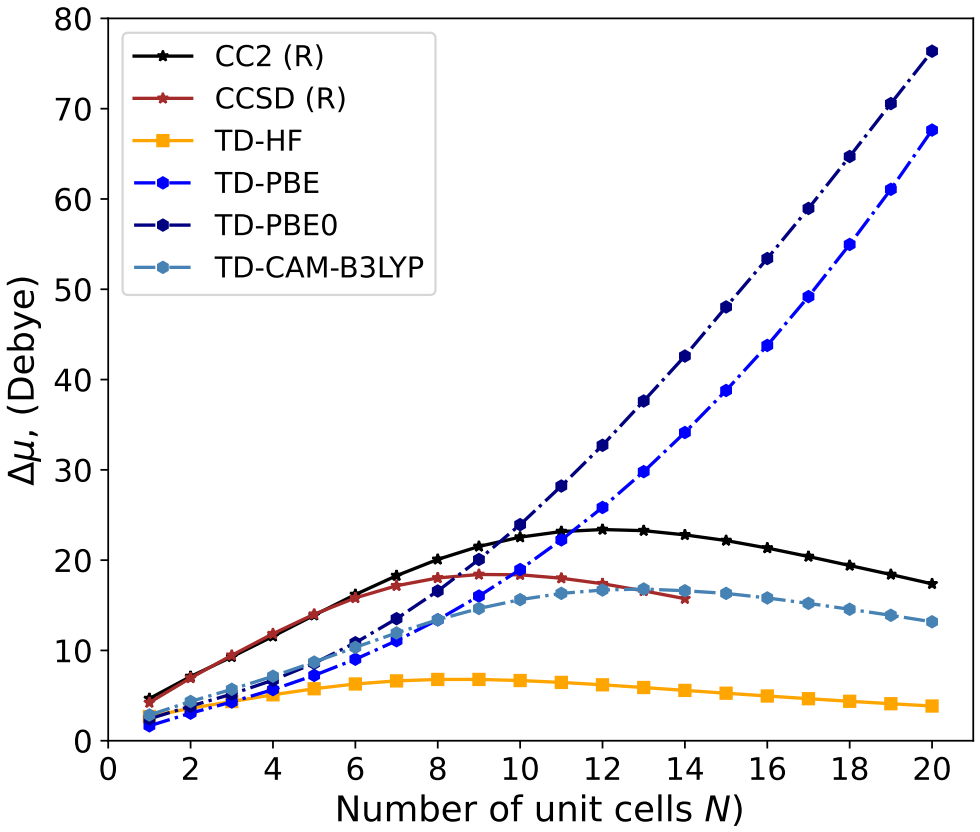

Figure 3: Evolution with N of $\Delta\mu$ obtained with TD-DFT/cc-pVTZ. See caption of Fig. 2 for more details. Note the different Y scales as compared to Fig. 2.

In Figure 3 we compare TD-DFT results obtained with three XCF to the relaxed CC2 and CCSD data presented above (see also Figure S3 in the SI for other properties). Both TD-PBE and TD-PBE0 incorrectly

predict $\Delta\mu$ (and μ^{ES}) constantly increasing with N, with very large values close to 70 D (100 D) for the eicosamer. This exaggeration trend is also present in μ^{GS}, though there is a clear saturation at large N for the GS property with both XCF (see Figure S3 in the SI). This unphysical behavior was already reported before by one of us for the same system with a smaller basis set.[15] TD-CAM-B3LYP that includes 65% of *exact* exchange at long-range cures the problem and provides a physically-sound topology with the a $\Delta\mu$ curve quite parallel to the CC2 one. As compared to the CCSD reference, one notes that the TD-CAM-B3LYP $\Delta\mu$ is peaking latter ($N = 13$ instead of $N = 9$) and at slightly lower value. This strongly XCF-dependent behavior of TD-DFT can be qualitatively explained by investigating electron density difference (EDD) plots displayed in Fig. 4 that indicates that: i) a CT from the amino towards the nitro group takes place for short chains with similar plots for all approaches for $N = 5$; ii) in longer oligomers both TD-CAM-B3LYP and TD-HF predict an excited state mainly localized at the center of the system; iii) for N=10 and 15, both TD-PBE and TD-PBE0 predicts a significant CT between the capping moieties, leading to more delocalized excited states than with TD-CAM-B3LYP . This is one illustration of the well-known TD-DFT problem for CT states when a semi-local XCF is used.[79,80] Finally, the interested reader can find comparisons between TD-DFT, CC2, and CCSD results for the ΔE and f in the SI, and both properties are strongly underestimated with both TD-PBE and TD-PBE0, as expected for CT systems.

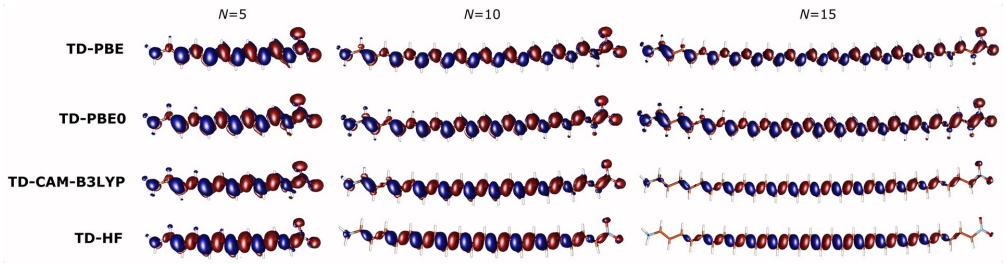

Figure 4: TD/cc-pVTZ electron density difference pots for three selected chain lengths and four approaches. The blue and red lobes correspond to decrease and increase of density upon polarization. Contour threshold: 0.001 au.

We now turn to BSE/*GW* results that were obtained through a finite-field difference numerical procedure, namely calculating numerically $\Delta\mu$ as the gradient of the BSE excitation energy with respect to a varying applied electric field (see the computational details and the SI for details). It is noteworthy that BSE calculations use the corresponding DFT values as μ^{GS}, so as to determine the μ^{ES} listed in the SI. The results are displayed in Figure 5 and show that irrespective of the selected XCF for the initial DFT calculations, BSE/ev*GW* provides very close estimates for $\Delta\mu$ for all chain lengths, in obvious contrast to the TD-DFT scenario. Strikingly, the maximal BSE/ev*GW* $\Delta\mu$ are almost perfectly equivalent: 12.0 D at $N = 10$ with

PBE, 12.3 D at $N = 10$ with PBE0, and 13.1 D at $N = 9$ with CAM-B3LYP. While these values are ca. 5-6 D smaller than their CCSD counterpart (18.4 D), the position is accurate ($N = 9$ with CCSD). The stability of the BSE excess dipoles with respect to input KS MOs strongly suggest that for this family of systems, much more expensive fully self-consistent GW calculations will not induce sizable corrections on the scale of the differences observed between CC2, EOM-CCSD and the various TD-DFT data. As can be seen in the SI (Figure S4), both BSE/evGW/PBE0 and BSE/evGW/CAM-B3LYP also provide very close estimates for both μ^{ES} at all chain lengths, but the differences are significant with BSE/evGW/PBE which delivers an almost constant μ^{ES} between N=12 and 20. As can be deduced from the $\Delta\mu$ curves, this effects is however mainly related to inaccuracies of the GS PBE dipoles. While in principle GS total energies could be calculated using ACFDT techniques,[81,82] and thus by finite difference the BSE ground-state dipole moments, one notes that the difference between the GS dipoles are much smaller than between the ES dipoles, suggesting that trying to calculate consistently GS and ES dipoles at the BSE level will marginally affect our results while being clearly out of reach in terms of cost for these rather large systems. This is a stimulating perspective to improve the efficiency of existing BSE ACFDT formalisms to explore GS dipoles. In short, one notices that, as for transition energies, the evGW procedure is very effective at washing out the deleterious XCF-dependency that plagues TD-DFT's results.

The very large underestimation of the TD-HF $\Delta\mu$, and to a lesser extent that of the BSE/evGW calculations, points to a possible underscreening of the electron-hole interaction in the self-consistent BSE/evGW calculations, reducing too strongly the average electron-hole distance. Using as an alternative the W_0 potential built from the Kohn-Sham PBE0 independent electron susceptibility, a scheme that we label BSE(W_0)/evGW/PBE0, one obtains a larger $\Delta\mu$ in closer agreement with the CC data. Such a result is consistent with the idea that building the W_0 BSE kernel from the smaller Kohn-Sham PBE0 gap, instead of the evGW one, leads to an increased screening. However the effect is somehow marginal and an underestimation pertains. Going now to the non-self-consistent BSE/G_0W_0/PBE0, where the diagonal BSE Hamiltonian is further built from single-shot G_0W_0 quasiparticle energies rather than the evGW quasiparticle energies, one obtains significantly larger excess dipoles, preserving however the qualitatively correct plateau and decay of $\Delta\mu$, albeit for longer N. This points to the importance as well of the occupied-to-virtual energy difference gradients in controlling the proper magnitude of the change of dipole in the excited state. Whatever Kohn-Sham starting point and BSE/GW scheme selected, we conclude that the BSE/GW scheme provides very reliable trends in the calculation of the ES dipoles, in contrast with TD-DFT calculations.

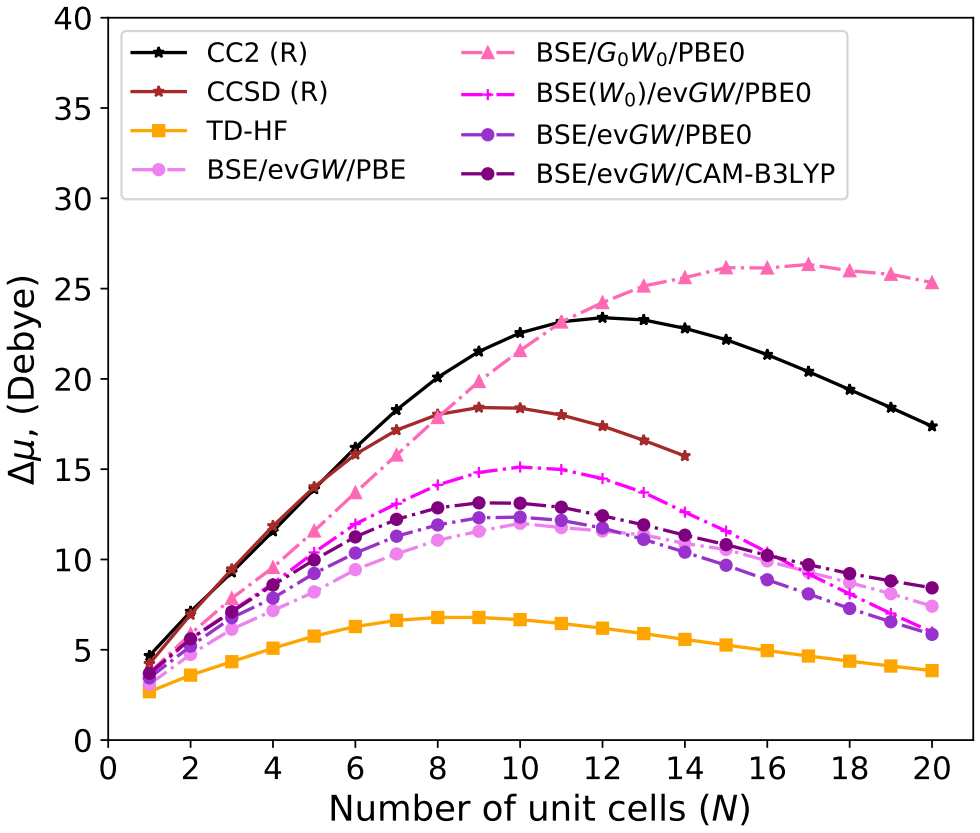

Figure 5: Evolution with N of $\Delta\mu$ obtained with BSE/GW and the cc-pVTZ basis set. See caption of Fig. 2 for more details.

Finally, let us compare TD-CAM-B3LYP to its BSE/evGW counterpart, which is done in Figure 6 and Figure S5 in the SI. As can be seen, for the excess dipole, the BSE/evGW curve is parallel to the CCSD one with an accurately located maximum, albeit with too small absolute values, as discussed above. In contrast, the TD-CAM-B3LYP $\Delta\mu$ seems to increase too slowly for short chains and saturate later, but with a maximal value close to the CCSD one. In some sense, BSE yields trends similar to CCSD, and TD-CAM-B3LYP closer to CC2, so both can be viewed as rather accurate.

In summary, we have investigated the evolution with chain length of the (ground and) excited state dipole moments of increasingly long push-pull chains using a panel of theoretical approaches, including wave function methods, time-dependent density functional theory, and Bethe-Salpeter equation formalisms, the two latter starting with three different exchange-correlation functionals. The electron correlated wave function schemes all show a fast increase of the excess dipole moment with chain length for the shortest chains, a maximum close to 10 ethynyl units, followed by a rather slow decrease. This trend is chemically sound. Indeed, as the donor amino and accepting nitro moieties become more distant, the magnitude of

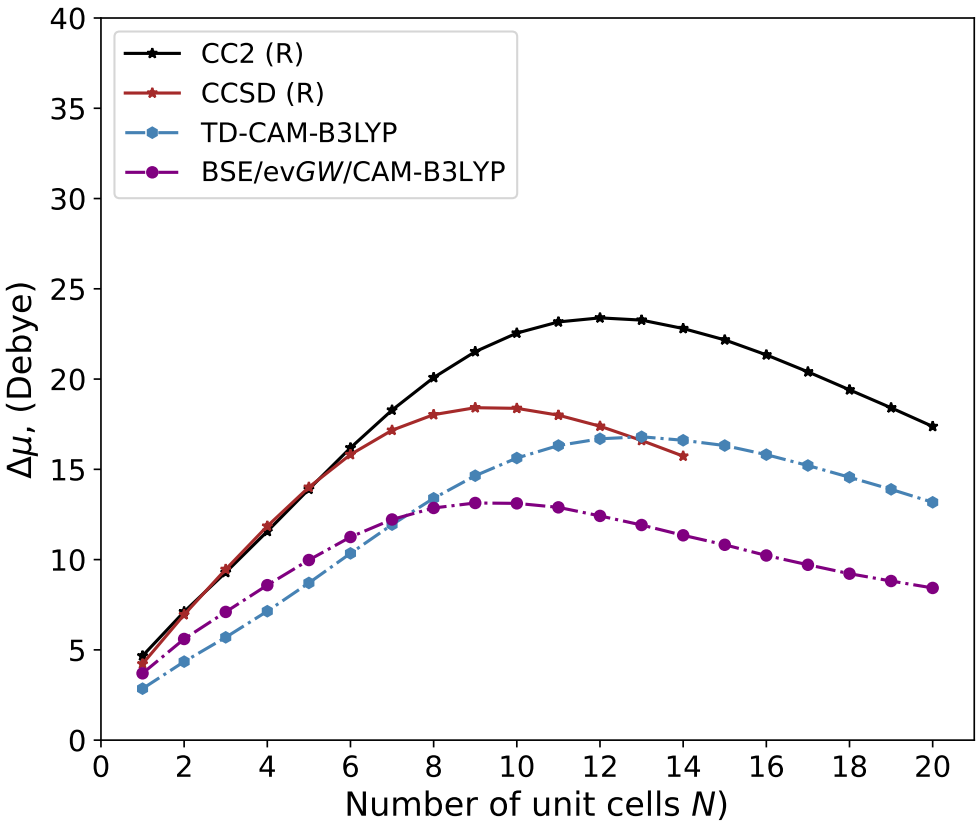

Figure 6: Evolution with N of $\Delta\mu$ obtained with selected methods. See caption of Fig. 2 for more details.

the photoinduced CT from the former to the latter first rapidly increases since the selected polyene units offer an ideal π-conjugated bridge. Nevertheless, for very long chains the electron "jump" from the amine to the nitro group becomes beyond reach on the lowest excited state, and the corresponding electronic transition becomes more localized on the polyene bridge, the terminal groups becoming passive elements in the transition. This subtle balance between delocalization, CT strength, and chain length undoubtedly constitutes a stringent benchmark for all theories, and one indeed notices non-trifling differences between the CC2 and CCSD results, the latter providing a lower maximal $\Delta\mu$ appearing for shorter oligomers as compared to the former method. At the TD-DFT level, both PBE and PBE0 deliver totally incorrect trends, a striking illustration of the failure of this XCF for long-range CT. TD-CAM-B3LYP allows restoring a qualitatively-accurate behavior, but the maximal $\Delta\mu$ is displaced to $N = 13$ instead of $N = 9$ with CCSD. In sharp contrast, BSE/evGW delivers $\Delta\mu$ presenting the physically-correct trends, as well as peaking at an accurate system size. Yet, these excess dipole moments appear to be too low by ca. 30% as compared to the best wave function approaches that can be used. On the contrary, non-self-consistent BSE/G_0W_0@PBE0

slightly overshoots the excess dipole, indicating that a more systematic exploration of the different levels of self-consistency may help better understanding the merits of the BSE excited states dipoles. It is our hope that the present contribution, demonstrating the abilities of BSE/evGW beyond transition energies and oscillator strengths, will stimulate further evaluations as well as extra developments, especially the derivation of analytical BSE/GW gradients.

COMPUTATIONAL DETAILS

The GS geometry of the $N = 1$–15 chains have been taken from Ref. 15, while the structure of longer chains has been consistently determined at the the M06-2X/6-31+G(d) level[83] with the Gaussian16.A.03 code[84] enforcing the C_s symmetry. All calculations use the same geometries, with Cartesian coordinates available in the SI. All TD-DFT calculations have been performed with Gaussian16, using the cc-pVTZ atomic basis set and three XCF, namely PBE,[85] PBE0,[86,87] and CAM-B3LYP,[88] as representatives of a semi-local GGA, a typical global hybrid, and a popular range-separated hybrid, respectively. These calculations used Gaussian16 default procedures and algorithms, but for a *tight* geometry optimization threshold. Both ADC(2) and CC2 calculations have been performed with the same cc-pVTZ basis set using the Turbomole 7.3 code[89,90] and systematically applying default convergence options, but for the use of the resolution-of-identity (RI) approach[91] and the frozen-core option. These ADC(2) and CC2 calculations have been achieved within the LR formalism and both the unrelaxed and relaxed schemes were used. The orbital relaxed EOM-CCSD calculations have been determined with the Q-Chem 6.0.1 code,[92] using both the cc-pVDZ and cc-pVTZ atomic basis sets combined with the corresponding RI basis set. The larger basis could be applied for the shortest chains only for obvious computational reasons. In these Q-Chem calculations, the core electrons were frozen and the following parameters were tightened to ensure numerical accuracy: i) the SCF convergence was set to 10^{-11}; ii) the CC GS convergence to 10^{-9}; iii) the integral threshold was set to 10^{-14}; iv) the EOM-CCSD convergence was set to 10^{-7}; and v) the Davidson diagonalization threshold was set to 10^{-5}. It is noteworthy that all TD-DFT, ADC(2), CC2, and CCSD calculations rely on analytical implementations for determining the μ^{ES}. The BSE/GW calculations were performed with the beDeft (beyondDFT) package[93] implementing Coulomb-fitting RI techniques[94] and an improved robust analytic continuation approach to GW dynamical correlations. The BSE/GW dipole moments were determined using the finite field difference method. We applied the electric field of ±0.000125 and ±0.00025 a.u. along the three Cartesian axis (see the SI for more information and numerical tests). This was achieved for the GS

calculation using ORCA 5.1 program[95] and the obtained Kohn-Sham eigenstates were used for the following beDeft BSE/*GW* calculations. The initial Kohn-Sham results have been obtained with PBE,[85] PBE0,[86] and CAM-B3LYP[88] exchange-correlation functionals. We used several schemes at the *GW* level including G_0W_0, the partially self-consistent ev*GW*, and the above-described BSE(W_0)/ev*GW*. At the *GW* level, we corrected 3 highest occupied and the 3 lowest unoccupied eigenvalues, except few cases as explained in the SI. We estimated the BSE/*GW* dipole moments using the five-point numerical derivative as well as other technics to approximate the first-order derivatives (see the SI for more details). In all cases, the excess dipole moments were determined from their GS and ES counterparts using:[15]

$$\Delta\mu = \sqrt{\left(\mu_x^{\mathrm{ES}} - \mu_x^{\mathrm{GS}}\right)^2 + \left(\mu_y^{\mathrm{ES}} - \mu_y^{\mathrm{GS}}\right)^2 + \left(\mu_z^{\mathrm{ES}} - \mu_z^{\mathrm{GS}}\right)^2} \tag{1}$$

In the present case, the absolute magnitude of the ES dipole is always larger than that of the GS dipole.

ACKNOWLEDGMENTS

The authors are indebted to the French Agence Nationale de la Recherche (ANR) under contract ANR-20-CE29-0005 (BSE-Forces) for financial support. I.K. and D.J. are indebted to the EUR LUMOMAT program and the Investments for the Future program (contract ANR-18-EURE-0012) for support. The authors are thankful for the generous allocations of time by the CCIPL computational center installed in Nantes and by the national HPC facilities (contract GENCI-TGCC A0110910016).

SUPPORTING INFORMATION AVAILABLE

Full list of numerical results. Basis set effects at CCSD level. Additional technical details for BSE calculations. Cartesian coordinates.

REFERENCES

(1) Lombardi, J. R. On the Comparison of Solvatochromic Shifts with Gas Phase Stark Effect Measurements. *Spectrochim. Acta A* **1987**, *43*, 1323–1324.

(2) Schmitt, M.; Meerts, L. In *Frontiers and Advances in Molecular Spectroscopy*; Laane, J., Ed.; Elsevier, 2018; Chapter 5, pp 143–193.

(3) Sarkar, R.; Boggio-Pasqua, M.; Loos, P.-F.; Jacquemin, D. Benchmarking TD-DFT and Wave Function

Methods for Oscillator Strengths and Excited-State Dipole Moments. *J. Chem. Theory Comput.* **2021**, *17*, 1117–1132.

(4) Runge, E.; Gross, E. K. U. Density-Functional Theory for Time-Dependent Systems. *Phys. Rev. Lett.* **1984**, *52*, 997–1000.

(5) Casida, M. E. In *Time-Dependent Density-Functional Response Theory for Molecules*; Chong, D. P., Ed.; Recent Advances in Density Functional Methods; World Scientific: Singapore, 1995; Vol. 1; pp 155–192.

(6) Adamo, C.; Jacquemin, D. The calculations of Excited-State Properties with Time-Dependent Density Functional Theory. *Chem. Soc. Rev.* **2013**, *42*, 845–856.

(7) van Caillie, C.; Amos, R. D. Geometric Derivatives of Density Functional Theory Excitation Energies Using Gradient-Corrected Functionals. *Chem. Phys. Lett.* **2000**, *317*, 159–164.

(8) Furche, F.; Ahlrichs, R. Adiabatic Time-Dependent Density Functional Methods for Excited States Properties. *J. Chem. Phys.* **2002**, *117*, 7433–7447.

(9) King, R. A. On the Accuracy of Computed Excited-State Dipole Moments. *J. Phys. Chem. A* **2008**, *112*, 5727–5733.

(10) Silva-Junior, M. R.; Schreiber, M.; Sauer, S. P. A.; Thiel, W. Benchmarks for Electronically Excited States: Time-Dependent Density Functional Theory and Density Functional Theory Based Multireference Configuration Interaction. *J. Chem. Phys.* **2008**, *129*, 104103.

(11) Wong, B. M.; Piacenza, M.; Della Sala, F. Absorption and Fluorescence Properties of Oligothiophene Biomarkers from Long-Range-Corrected Absorption and Fluorescence Properties of Oligothiophene Biomarkersfrom Long-Range-Corrected Time-Dependent Density Functional Theory. *Phys. Chem. Chem. Phys.* **2009**, *11*, 4498–4508.

(12) Tapavicza, E.; Tavernelli, I.; Rothlisberger, U. Ab Initio Excited State Properties and Dynamics of a Prototype σ-Bridged-Donor-Acceptor Molecule. *J. Phys. Chem. A* **2009**, *113*, 9595–9602.

(13) Guido, C. A.; Jacquemin, D.; Adamo, C.; Mennucci, B. On the TD-DFT Accuracy in Determining Single and Double Bonds in Excited-State Structures of Organic Molecules. *J. Phys. Chem. A* **2010**, *114*, 13402–13410.

(14) Silva-Junior, M. R.; Thiel, W. Benchmark of Electronically Excited States for Semiempirical Methods: MNDO, AM1, PM3, OM1, OM2, OM3, INDO/S, and INDO/S2. *J. Chem. Theory Comput.* **2010**, *6*, 1546–1564.

(15) Jacquemin, D. Excited-State Dipole and Quadrupole Moments: TD-DFT versus CC2. *J. Chem. Theory Comput.* **2016**, *12*, 3993–4003.

(16) Hait, D.; Head-Gordon, M. How Accurate Is Density Functional Theory at Predicting Dipole Moments? An Assessment Using a New Database of 200 Benchmark Values. *J. Chem. Theory Comput.* **2018**, *14*, 1969–1981.

(17) Hait, D.; Liang, Y. H.; Head-Gordon, M. Too Big, Too Small or Just Right? A Benchmark Assessment of Density Functional Theory for Predicting ehe Spatial Extent of the Electron Density of Small Chemical Systems. **2020**, arXiv:2011.12561.

(18) Christiansen, O.; Koch, H.; Jørgensen, P. The Second-Order Approximate Coupled Cluster Singles and Doubles Model CC2. *Chem. Phys. Lett.* **1995**, *243*, 409–418.

(19) Schirmer, J. Beyond the Random-Phase Approximation: a new Approximation Scheme for the Polarization Propagator. *Phys. Rev. A* **1982**, *26*, 2395–2416.

(20) Dreuw, A.; Wormit, M. The Algebraic Diagrammatic Construction Scheme for the Polarization Propagator for the Calculation of Excited States. *WIREs Comput. Mol. Sci.* **2015**, *5*, 82–95.

(21) Hellweg, A. The Accuracy of Dipole Moments from Spin-Component Scaled CC2 in Ground and Electronically Excited States. *J. Chem. Phys.* **2011**, *134*, 064103.

(22) Hodecker, M.; Rehn, D. R.; Dreuw, A.; Höfener, S. Similarities and Differences of the Lagrange Formalism and the Intermediate State Representation in the Treatment of Molecular Properties. *J. Chem. Phys.* **2019**, *150*, 164125.

(23) Hodecker, M.; Dreuw, A. Unitary Coupled Cluster Ground- and Excited-State Molecular Properties. *J. Chem. Phys.* **2020**, *153*, 084112.

(24) Helgaker, T.; Jørgensen, P.; Handy, N. A Numerically Stable Procedure for Calculating Møller-Plesset Energy Derivatives, Derived Using the Theory of Lagrangians. *Theoret. Chim. Acta* **1989**, *76*, 227–245.

(25) Koch, H.; Jensen, H. J. A.; Jorgensen, P.; Helgaker, T.; Scuseria, G. E.; Schaefer, H. F. Coupled Cluster Energy Derivatives. Analytic Hessian for the Closed?Shell Coupled Cluster Singles and Doubles Wave Function: Theory and Applications. *J. Chem. Phys.* **1990**, *92*, 4924–4940.

(26) Christiansen, O.; Jørgensen, P.; Hättig, C. Response Functions from Fourier Component Variational Perturbation Theory Applied to a Time-Averaged Quasienergy. *Int. J. Quantum Chem.* **1998**, *68*, 1–52.

(27) Hättig, C. Geometry Optimizations with the Coupled-Cluster Model CC2 Using the Resolution-of-the-Identity Approximation. *J. Chem. Phys.* **2003**, *118*, 7751–7761.

(28) Kállay, M.; Gauss, J. Calculation of Excited-State Properties Using General Coupled-Cluster and Configuration-Interaction Models. *J. Chem. Phys.* **2004**, *121*, 9257–9269.

(29) Hättig, C. In *Response Theory and Molecular Properties (A Tribute to Jan Linderberg and Poul Jørgensen)*; Jensen, H. A., Ed.; Advances in Quantum Chemistry; Academic Press: Amsterdam, Boston, Heidelberg, 2005; Vol. 50; pp 37–60.

(30) Salter, E. A.; Sekino, H.; Bartlett, R. J. Property Evaluation and Orbital Relaxation in Coupled Cluster Methods. *J. Chem. Phys.* **1987**, *87*, 502–509.

(31) Trucks, G. W.; Salter, E.; Sosa, C.; Bartlett, R. J. Theory and Implementation of the MBPT Density Matrix. An Application to One-Electron Properties. *Chem. Phys. Lett.* **1988**, *147*, 359–366.

(32) Schirmer, J. Closed-Form Intermediate Representations of Many-Body Propagators and Resolvent Matrices. *Phys. Rev. A.* **1991**, *43*, 4647–4659.

(33) Schirmer, J.; Mertins, F. Review of Biorthogonal Coupled Cluster Representations for Electronic Excitation. *Theor. Chem. Acc.* **2010**, *125*, 145–172.

(34) Rowe, D. J. Equations-of-Motion Method and the Extended Shell Model. *Rev. Mod. Phys.* **1968**, *40*, 153–166.

(35) Stanton, J. F.; Bartlett, R. J. The Equation of Motion Coupled-Cluster Method - A Systematic Biorthogonal Approach to Molecular Excitation Energies, Transition-Probabilities, and Excited-State Properties. *J. Chem. Phys.* **1993**, *98*, 7029–7039.

(36) Koch, H.; Kobayashi, R.; Sanchez de Merás, A.; Jorgensen, P. Calculation of Size?Intensive Transition Moments from the Coupled Cluster Singles and Doubles Linear Response Function. *J. Chem. Phys.* **1994**, *100*, 4393–4400.

(37) Salpeter, E. E.; Bethe, H. A. A Relativistic Equation for Bound-State Problems. *Phys. Rev.* **1951**, *84*, 1232–1242.

(38) Csanak, G.; Taylor, H.; Yaris, R. In *Advances in Atomic and Molecular Physics*; Bates, D., Esterman, I., Eds.; Advances in Atomic and Molecular Physics; Academic Press: Amsterdam, Boston, Heidelberg, 1971; Vol. 7; pp 287–361.

(39) Hanke, W.; Sham, L. J. Many-Particle Effects in the Optical Excitations of a Semiconductor. *Phys. Rev. Lett.* **1979**, *43*, 387–390.

(40) Strinati, G. Application of the Green's Functions Method to the Study of the Optical Properties of Semiconductors. *Riv. Nuovo Cimento* **1988**, *11*, 1–86.

(41) Rohlfing, M.; Louie, S. G. Excitonic Effects and the Optical Absorption Spectrum of Hydrogenated Si Clusters. *Phys. Rev. Lett.* **1998**, *80*, 3320–3323.

(42) Albrecht, S.; Reining, L.; Del Sole, R.; Onida, G. *Ab Initio* Calculation of Excitonic Effects in the Optical Spectra of Semiconductors. *Phys. Rev. Lett.* **1998**, *80*, 4510–4513.

(43) Benedict, L. X.; Shirley, E. L.; Bohn, R. B. Optical Absorption of Insulators and the Electron-Hole Interaction: An *Ab Initio* Calculation. *Phys. Rev. Lett.* **1998**, *80*, 4514–4517.

(44) Martin, R. M.; Reining, L.; Ceperley, D. M. *Interacting electrons: Theory and computational approaches*; Cambridge University Press: Cambridge, 2016.

(45) Blase, X.; Duchemin, I.; Jacquemin, D. The Bethe-Salpeter Equation in Chemistry: Relations with TD-DFT, Applications and Challenges. *Chem. Soc. Rev.* **2018**, *47*, 1022–1043.

(46) Blase, X.; Duchemin, I.; Jacquemin, D.; Loos, P.-F. The Bethe–Salpeter Equation Formalism: From Physics to Chemistry. *J. Phys. Chem. Lett.* **2020**, *11*, 7371–7382.

(47) Hedin, L. New Method for Calculating the One-Particle Green's Function with Application to the Electron-Gas Problem. *Phys. Rev. A* **1965**, *139*, 796–823.

(48) Strinati, G.; Mattausch, H.; Hanke, W. Dynamical Correlation Effects on the Quasiparticle Bloch States of a Covalent Crystal. *Phys. Rev. Lett.* **1980**, *45*, 290–294.

(49) Hybertsen, M. S.; Louie, S. G. Electron Correlation in Semiconductors and Insulators: Band Gaps and Quasiparticle Energies. *Phys. Rev. B* **1986**, *34*, 5390–5413.

(50) Godby, R. W.; Schlüter, M.; Sham, L. J. Self-Energy Operators and Exchange-Correlation Potentials in Semiconductors. *Phys. Rev. B* **1988**, *37*, 10159–10175.

(51) Golze, D.; Dvorak, M.; Rinke, P. The *GW* Compendium: A Practical Guide to Theoretical Photoemission Spectroscopy. *Front. Chem.* **2019**, *7*, 377.

(52) Rocca, D.; Lu, D.; Galli, G. Ab Initio Calculations of Optical Absorption Spectra: Solution of the Bethe–Salpeter Equation Within Density Matrix Perturbation Theory. *J. Chem. Phys.* **2010**, *133*, 164109.

(53) Blase, X.; Attaccalite, C. Charge-Transfer Excitations in Molecular Donor-Acceptor Complexes Within the Many-Body Bethe-Salpeter Approach. *Appl. Phys. Lett.* **2011**, *99*, 171909.

(54) Baumeier, B.; Andrienko, D.; Rohlfing, M. Frenkel and Charge-Transfer Excitations in Donor–acceptor Complexes from Many-Body Green's Functions Theory. *J. Chem. Theory Comput.* **2012**, *8*, 2790–2795.

(55) Cudazzo, P.; Gatti, M.; Rubio, A.; Sottile, F. Frenkel *versus* Charge-Transfer Exciton Dispersion in Molecular Crystals. *Phys. Rev. B* **2013**, *88*, 195152.

(56) Ziaei, V.; Bredow, T. GW-BSE Approach on S1 Vertical Transition Energy of Large Charge Transfer Compounds: A Performance Assessment. *J. Chem. Phys.* **2016**, *145*, 174305.

(57) Jacquemin, D.; Duchemin, I.; Blase, X. Benchmarking the Bethe-Salpeter Formalism on a Standard Organic Molecular Set. *J. Chem. Theory Comput.* **2015**, *11*, 3290–3304.

(58) Jacquemin, D.; Duchemin, I.; Blase, X. 0–0 Energies Using Hybrid Schemes: Benchmarks of TD-DFT, CIS(D), ADC(2), CC2, and BSE/GW formalisms for 80 Real-Life Compounds. *J. Chem. Theory Comput.* **2015**, *11*, 5340–5359.

(59) Bruneval, F.; Hamed, S. M.; Neaton, J. B. A Systematic Benchmark of the Ab Initio Bethe-Salpeter Equation Approach for Low-Lying Optical Excitations of Small Organic Molecules. *J. Chem. Phys.* **2015**, *142*, 244101.

(60) Krause, K.; Klopper, W. Implementation of the Bethe-Salpeter Equation in the TURBOMOLE Program. *J. Comput. Chem.* **2017**, *38*, 383–388.

(61) Jacquemin, D.; Duchemin, I.; Blase, X. Is the Bethe–Salpeter Formalism Accurate for Excitation Energies? Comparisons with TD-DFT, CASPT2, and EOM-CCSD. *J. Phys. Chem. Lett.* **2017**, *8*, 1524–1529.

(62) Rangel, T.; Hamed, S. M.; Bruneval, F.; Neaton, J. B. An Assessment of Low-Lying Excitation Energies and Triplet Instabilities of Organic Molecules With an Ab Initio Bethe-Salpeter Equation Approach and the Tamm-Dancoff Approximation. *J. Chem. Phys.* **2017**, *146*, 194108.

(63) Gui, X.; Holzer, C.; Klopper, W. Accuracy Assessment of *GW* Starting Points for Calculating Molecular Excitation Energies Using the Bethe–Salpeter Formalism. *J. Chem. Theory Comput.* **2018**, *14*, 2127–2136.

(64) Nguyen, N. L.; Ma, H.; Govoni, M.; Gygi, F.; Galli, G. Finite-Field Approach to Solving the Bethe-Salpeter Equation. *Phys. Rev. Lett.* **2019**, *122*, 237402.

(65) Liu, C.; Kloppenburg, J.; Yao, Y.; Ren, X.; Appel, H.; Kanai, Y.; Blum, V. All-Electron ab initio Bethe-Salpeter Equation Approach to Neutral Excitations in Molecules with Numeric Atom-Centered Orbitals. *J. Chem. Phys.* **2020**, *152*, 044105.

(66) Li, J.; Golze, D.; Yang, W. Combining Renormalized Singles GW Methods with the Bethe–Salpeter Equation for Accurate Neutral Excitation Energies. *J. Chem. Theory Comput.* **2022**, *18*, 6637–6645.

(67) McKeon, C. A.; Hamed, S. M.; Bruneval, F.; Neaton, J. B. An Optimally Tuned Range-Separated Hybrid Starting Point for ab initio *GW* plus Bethe–Salpeter Equation Calculations of Molecules. *J. Chem. Phys.* **2022**, *157*, 074103.

(68) Shishkin, M.; Kresse, G. Self-Consistent GW Calculations for Semiconductors and Insulators. *Phys. Rev. B* **2007**, *75*, 235102.

(69) Rangel, T.; Hamed, S. M.; Bruneval, F.; Neaton, J. B. Evaluating the *GW* Approximation with CCSD(T) for Charged Excitations Across the Oligoacenes. *J. Chem. Theory Comput.* **2016**, *12*, 2834–2842.

(70) Kaplan, F.; Harding, M. E.; Seiler, C.; Weigend, F.; Evers, F.; van Setten, M. J. Quasi-Particle Self-Consistent *GW* for Molecules. *J. Chem. Theory Comput.* **2016**, *12*, 2528–2541.

(71) Jacquemin, D.; Duchemin, I.; Blondel, A.; Blase, X. Assessment of the Accuracy of the Bethe-Salpeter (BSE/GW) Oscillator Strengths. *J. Chem. Theory Comput.* **2016**, *12*, 3969–3981.

(72) Kaczmarski, M. S.; Rohlfing, M. Diabatic Electronic States from Many-Body Perturbation Theory. *J. Phys. B: At. Mol. Opt. Phys.* **2010**, *43*, 051001.

(73) Çaylak, O.; Baumeier, B. Excited-State Geometry Optimization of Small Molecules with Many-Body Green's Functions Theory. *J. Chem. Theory Comput.* **2021**, *17*, 879–888.

(74) Ismail-Beigi, S.; Louie, S. G. Excited-State Forces Within a First-Principle Green's Function Formalism. *Phys. Rev. Lett.* **2003**, *90*, 076401.

(75) Kaczmarski, M. S.; Ma, Y.; Rohlfing, M. Diabatic States of a Photoexcited Retinal Chromophore from ab initio Many-Body Perturbation Theory. *Phys. Rev. B* **2010**, *81*, 115433.

(76) Knysh, I.; Duchemin, I.; Blase, X.; Jacquemin, D. Modeling of Excited State Potential Energy Surfaces with the Bethe–Salpeter Equation Formalism: The 4-(Dimethylamino)benzonitrile Twist. *J. Chem. Phys.* **2022**, *157*, 194102.

(77) Knysh, I.; Letellier, K.; Duchemin, I.; Blase, X.; Jacquemin, D. Excited State Potential Energy Surfaces of N-Phenylpyrrole upon Twisting: Reference calues and Comparison Between BSE/GW and TD-DFT. *Phys. Chem. Chem. Phys.* **2023**, *25*, 8376–8385.

(78) Véril, M.; Scemama, A.; Caffarel, M.; Lipparini, F.; Boggio-Pasqua, M.; Jacquemin, D.; Loos, P.-F. QUESTDB: a Database of Highly-Accurate Excitation Energies for the Electronic Structure Community. *WIREs Comput. Mol. Sci.* **2021**, *11*, e1517.

(79) Tozer, D. J. Relationship Between Long-Range Charge-Transfer Excitation Energy Error and Integer Discontinuity in Kohn-Sham Theory. *J. Chem. Phys.* **2003**, *119*, 12697–12699.

(80) Dreuw, A.; Head-Gordon, M. Failure of Time-Dependent Density Functional Theory for Long-Range Charge-Transfer Excited States: the Zincbacteriochlorin-Bacteriochlorin and Bacteriochlorophyll-Spheroidene Complexes. *J. Am. Chem. Soc.* **2004**, *126*, 4007–4016.

(81) Holzer, C.; Gui, X.; Harding, M. E.; Kresse, G.; Helgaker, T.; Klopper, W. Bethe–Salpeter Correlation Energies of Atoms and Molecules. *J. Chem. Phys.* **2018**, *149*, 144106.

(82) Loos, P.-F.; Scemama, A.; Duchemin, I.; Jacquemin, D.; Blase, X. Pros and Cons of the Bethe–Salpeter Formalism for Ground-State Energies. *J. Phys. Chem. Lett.* **2020**, *11*, 3536–3545.

(83) Zhao, Y.; Truhlar, D. G. The M06 Suite of Density Functionals for Main Group Thermochemistry, Thermochemical Kinetics, Noncovalent Interactions, Excited States, and Transition Elements: Two New Functionals and Systematic Testing of Four M06-Class Functionals and 12 Other Functionals. *Theor. Chem. Acc.* **2008**, *120*, 215–241.

(84) Frisch, M. J.; Trucks, G. W.; Schlegel, H. B.; Scuseria, G. E.; Robb, M. A.; Cheeseman, J. R.; Scalmani, G.; Barone, V.; Petersson, G. A.; Nakatsuji, H. et al. Gaussian 16 Revision A.03. 2016; Gaussian Inc. Wallingford CT.

(85) Perdew, J. P.; Burke, K.; Ernzerhof, M. Generalized Gradient Approximation Made Simple. *Phys. Rev. Lett.* **1996**, *77*, 3865–3868.

(86) Adamo, C.; Barone, V. Toward Reliable Density Functional Methods Without Adjustable Parameters: the PBE0 Model. *J. Chem. Phys.* **1999**, *110*, 6158–6170.

(87) Ernzerhof, M.; Scuseria, G. E. Assessment of the Perdew–Burke–Ernzerhof Exchange-Correlation Functional. *J. Chem. Phys.* **1999**, *110*, 5029–5036.

(88) Yanai, T.; Tew, D. P.; Handy, N. C. A New Hybrid Exchange-Correlation Functional Using the Coulomb-Attenuating Method (CAM-B3LYP). *Chem. Phys. Lett.* **2004**, *393*, 51–56.

(89) Balasubramani, S. G.; Chen, G. P.; Coriani, S.; Diedenhofen, M.; Frank, M. S.; Franzke, Y. J.; Furche, F.; Grotjahn, R.; Harding, M. E.; Hättig, C. et al. TURBOMOLE: Modular Program Suite for ab initio Quantum-Chemical and Condensed-Matter Simulations. *J. Chem. Phys.* **2020**, *152*, 184107.

(90) TURBOMOLE V7.3 2018, a development of University of Karlsruhe and Forschungszentrum Karlsruhe GmbH, 1989-2007, TURBOMOLE GmbH, since 2007.

(91) Hättig, C.; Weigend, F. CC2 Excitation Energy Calculations on Large Molecules Using the Resolution of the Identity Approximation. *J. Chem. Phys.* **2000**, *113*, 5154–5161.

(92) Epifanovsky, E.; Gilbert, A. T. B.; Feng, X.; Lee, J.; Mao, Y.; Mardirossian, N.; Pokhilko, P.;

White, A. F.; Coons, M. P.; Dempwolff, A. L. et al. Software for the Frontiers of Quantum Chemistry: An Overview of Developments in the Q-Chem 5 Package. *J. Chem. Phys.* **2021**, *155*, 084801.

(93) Duchemin, I.; Blase, X. Robust Analytic-Continuation Approach to Many-Body GW Calculations. *J. Chem. Theory Comput.* **2020**, *16*, 1742–1756.

(94) Ren, X.; Rinke, P.; Blum, V.; Wieferink, J.; Tkatchenko, A.; Sanfilippo, A.; Reuter, K.; Scheffler, M. Resolution-of-Identity Approach to Hartree–Fock, Hybrid Density Functionals, RPA, MP2 and GW with Numeric Atom-Centered Orbital Basis Functions. *New. J. Phys.* **2012**, *14*, 053020.

(95) Neese, F.; Wennmohs, F.; Becker, U.; Riplinger, C. The ORCA Quantum Chemistry Program Package. *J. Chem. Phys.* **2020**, *152*, 224108.